ACS OMEGA

http://pubs.acs.org/journal/acsodf

Article

Dual-Comb Gas Sensor Integrated with a Neural Network-Based Spectral Decoupling Algorithm of Overlapped Spectra for Gas Mixture Sensing

Qingjin Chi, Linbo Tian,* Rongqi Xu, Zhao Wang, Fengrong Zhao, Kegang Guo, Zhaowen Liang, Jinbao Xia, and Sasa Zhang*

Cite This: *ACS Omega* 2023, 8, 14648−14655

Read Online

ACCESS | Metrics & More | Article Recommendations | Supporting Information

ABSTRACT: Cross-interference among absorptions severely affects the ability to achieve accurate gas concentration retrieval through gas molecular specificity. In this study, a novel dual gas sensor was proposed to separate methane and water absorbance from the blended spectra of their mixture in the mid-infrared (MIR) band by employing a neural network algorithm. To address the scarcity of experimental data, the neural network was trained over a simulated data set constructed with the same distribution as the experimental ones. The system takes advantages of the broadband spectra to provide high-quality comb data and allows the neural network to establish an accurate spectral decoupling function. In addition, a feature absorption peak screening mechanism was proposed to achieve more accurate concentration retrieval, which avoids the prediction error introduced by interrogating the only peak of the separated spectra. The promising results of the systematic evaluation have demonstrated the feasibility of our methods in practical detections.

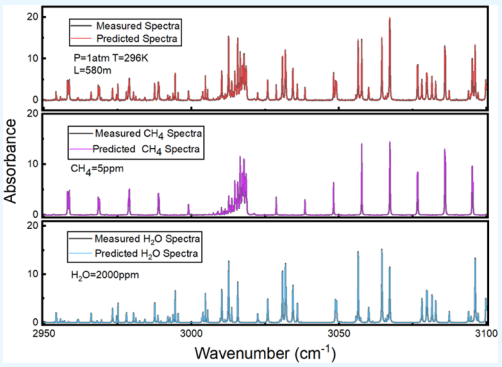

1. INTRODUCTION

Methane is the main component of natural gas and the second most important greenhouse gas after carbon dioxide.[1] Therefore, the accurate measurement of methane concentration is of great importance for industrial production and environmental protection.[2,3] At present, the mainstream methane gas detection technologies mainly include catalytic combustion,[4] electrochemical,[5] thermal conductivity,[6] and gas spectroscopy-based detection technologies.[7,8] Spectroscopic detection techniques are becoming increasingly popular among researchers because of their fast response, high selectivity, high sensitivity, and noninvasive real-time measurements.[9] Laser spectroscopy techniques include tunable diode laser absorption spectroscopy (TDLAS),[10] cavity decay spectroscopy (CRDS),[11] photoacoustic spectroscopy (PAS),[12] etc. After obtaining the spectra of the target molecules, the concentrations can be directly calculated by linear or nonlinear fitting of the spectra.[13] However, these methods are limited by the overlapping absorbance spectra of various components of the gas mixture.[7]

The collimated semiconductor lasers are well suited for sensitive detection of a specific molecule, especially when the absorption lines of different molecular species are separated. Considering the limited tuning range, different equipment may be required for different gas monitoring in gas mixtures. High-impact experiments have been carried out with the QCL-based 2f-WMS approach, confirming its efficiency in multicomponent gas sensing. The detection of multicomponent gas mixtures at ppbv can be achieved by selecting the right combination of laser. To address the nonlinearity of 2f-WMS at high concentrations, heterodyne phase-sensitive dispersion spectroscopy (HPSDS) is used to extend its linearity range to 20 ppmv without replacing the gas measurement cell or installing an additional gas dilution system.[14] However, with the increase of the number of species of gases of interest, multiple individual laser sources may be required to analyze the gas mixture and thus increase the complexity of the system.[15] Furthermore, it may not be possible to find the right wavelength of laser to overcome the gas cross-talk problem. Similarly, the developed methane detection techniques often require a drying treatment before detection because of the cross-interference introduced by the water vapor.[16] However, drying equipment need to be replaced periodically for a short period of time, which is undoubtedly time-consuming and a safety hazard.[17] Even so, it is difficult to eliminate the residual

Received: January 25, 2023
Accepted: March 24, 2023
Published: March 30, 2023

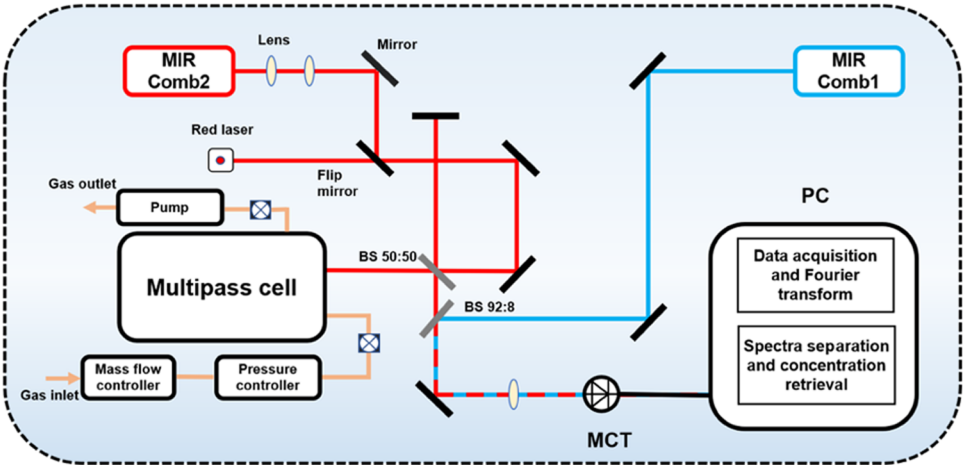

Figure 1. Schematic diagram of the experimental setup. Light from two MIR comb sources is coupled into the multipass cell (MPC) after passing through multiple lens and mirrors. One 50:50 beam splitter (BS) is used to split the reference and signal pulses, and the other one 92:8 BS is used to combine the pulses from the two combs. The pulses are eventually detected by an MCT photodetector and further processed by the computer.

water due to the material of the inner wall of the gas cell and improper operation.[18]

For simultaneous multicomponent gas detection, the problem of spectral cross-interference is still one of the difficulties that needs to be broken through.[19] Although mathematical methods such as Bayesian estimation and principal component analysis are used to solve cross-interference problems, strict conditions and a set of assumptions that cannot be realized in practical applications are often required, which can lead to less accurate predictions.[20,21] Least squares (LS) and partial least squares (PLS) are also of interest in resolving cross-interference.[22,23] The problem with such methods is that they cannot identify the species of a gas mixture from the corresponding blended spectra.[19] In contrast, Deep Learning, a better alternative, has developed rapidly in recent years and has widely been used in various fields because of its good performance and powerful capabilities to integrate with other scientific methods.[24] To date, deep learning algorithms, represented by various kinds of neural networks, have achieved impressive results in gas concentration retrieval,[7] spectral filtering,[25,26] hyperspectral imaging,[27] etc. However, the application of neural networks to solve the inherent problems of multicomponent gas mixtures with spectroscopy still needs to be urgently developed.

Based on the aforementioned background, a dual-comb spectrometer integrated with a neural network-based spectral decoupling algorithm was developed to overcome the widespread problem of water interference in methane detection of broadband MIR absorbance spectra. The proposed technique can directly separate the target specie and the interference one from the overlapping absorbance spectra, overcoming the challenge of light source selection when faced with too many gas species for QCL-based gas detection techniques, thus realizing the simultaneous direct detection of both molecules in the presence of interference without any preprocessing or additional equipment. The system includes a spectral acquisition module consisting of two DFG MIR high-power frequency comb sources, which are based on femtosecond Er:fiber oscillators with a stabilized repetition 105 rate at ∼250 MHz and a multipass cell (MPC) of ∼580 m interaction length. The high-quality comb data is analyzed by the spectral processing module (SPM) built by a well-optimized neural network. Through the training of a large amount of data, SPM learns to identify the respective contributions of methane and water vapor in the blended spectra and separate them precisely, thus solving the problem of cross-interference of water vapor to methane and realizing the long-term stable detection of methane. In Section 2, we have discussed the sensor configuration and the implementation of the SPM. Section 3 shows the results of SPM on the separation of blended spectra and the performance of the system in terms of concentration retrieval as well as the stability of measurements. The conclusive information and prospects for future work are talked about in Section 4.

2. METHODOLOGY

2.1. Sensor System Configuration. The spectral acquisition system uses two mid-infrared DFG frequency combs (Menlo Systems, MIR Comb) based on femtosecond erbium-doped fiber oscillators whose repetition rates are locked at ∼250 MHz and referenced to the Rb frequency standard (Stanford Research, PSR10). The output power of MIR Comb1 is about 120 mw, covering the spectral range of 2.8−3.6 μm, and the pulse duration is ∼80 fs. The MIR Comb2 employs a higher-power ytterbium-doped fiber amplifier that has a similar spectrum and pulse duration to the MIR Comb1 and produces a combined near-infrared beam of ∼300 mw. The volume of the MPC is 2.5 L. The two confocal mirrors have a radius of curvature of 1 m and are separated by 1 m. The conditions inside the cell are maintained stable by a flow controller and a pressure controller. After the laser beam is injected into the gas cell, it is reflected 579 times and then emitted, with an effective light path of 580 m.

After optical path calibration and mode matching, the laser beam emitted by the MIR Comb2 is split into two parts by a 50:50 beam splitter. One part serves as the transmission signal, consisting of signal pulses coupled to the MPC; the other part serves as the reference signal and then is guided back by the reflector. The transmitted signal is fully absorbed in the MPC and then recombined with the reference signal on the same 50:50 beam splitter and overlapped with the pulse from MIR comb1 on a 92:8 beam splitter. The combined pulses were focused on an HgCdTe (MCT) detector with a liquid nitrogen-cooled bandwidth of 100 MHz (Kolmar Technology,

https://doi.org/10.1021/acsomega.3c00518
ACS Omega 2023, 8, 14648−14655

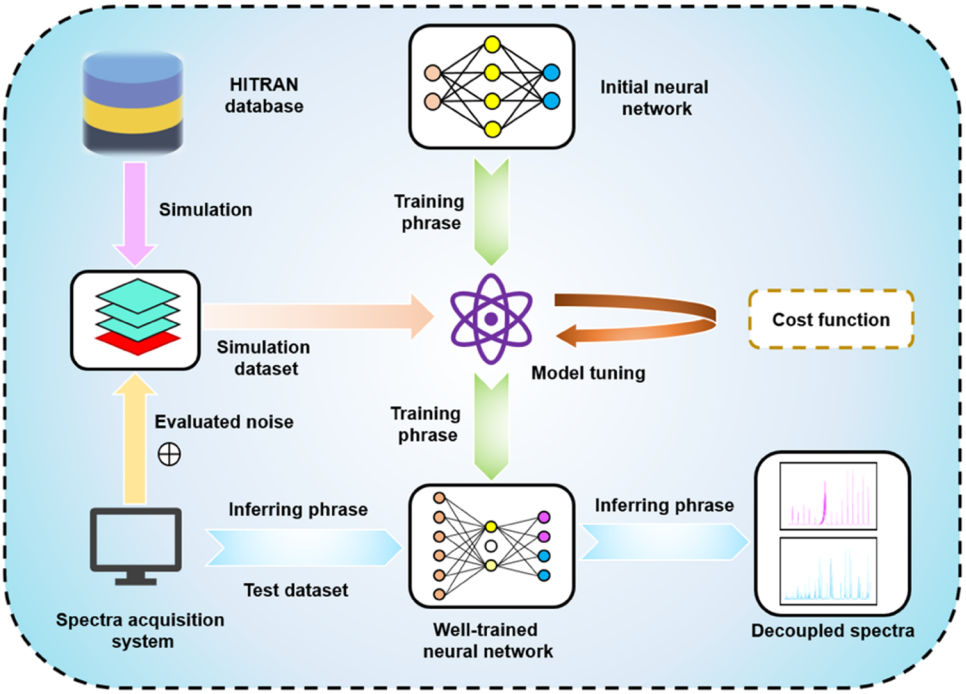

Figure 2. Flowchart of development of the blended absorption spectroscopy separation algorithm. The initial model is trained on a simulated data set. The well-trained neural network model is used to achieve accurate separation of the experimental data.

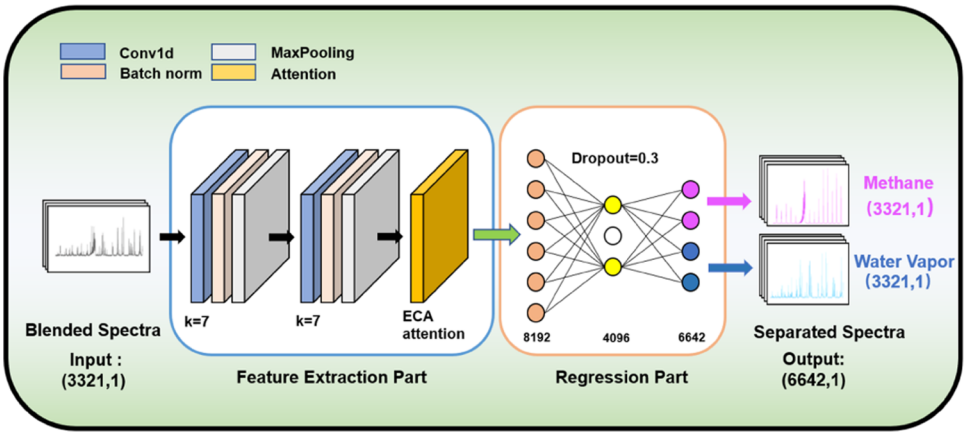

Figure 3. Neural network model structure. Abbreviations. k, kernel size. The blended spectra are fed into the model, and the separated gas spectra are output after processing by the feature extraction module and the spectral regression module.

KMPV11-0.1-J1/AC100). By using a filter and beam splitter, the total incident power on the detector is adjusted to be less than the detector saturation power of 2 mw. The optics setup is shown in Figure 1.

2.2. Data Sets. Neural networks as data processing and analysis algorithms are widely used in various fields because of their excellent performance. However, their superior performance relies on the quantity and quality of training data. In the field of gas absorption spectroscopy, it is time-consuming and labor-intensive to obtain sufficient data experimentally. Models trained on small amounts of data are limited in accuracy and sensitivity and often fail to demonstrate satisfactory results in the detection of trace gases. In this study, the solution to the data scarcity problem is to obtain the ideal absorption spectra of the gas mixtures under predefined experimental conditions from the HITRAN database and build the simulated data set by introducing systematic noises. This data augmentation strategy has been widely used in areas where information is scarce and has been proven to be practical [14]. Models trained on such simulated data sets will also perform well on experimental data.

From this perspective, we have obtained 15000 sets of absorption spectral data of methane and water vapor mixture with the conditions of P = 1 atm, T = 296 K, and path length = 580 m. Each simulated spectrum consists of 3321 sampling points for consistency according to the resolution of the experiment spectrum. The concentrations of methane and water vary randomly from 0 to 20 ppm and from 500 to 3000 ppm, respectively. After the evaluation of the system, system noise was introduced to the simulated spectra to make the distribution closer to that of the experimental ones and increase the robustness of the model to unexpected disturbances. In this task, the separation of the blended spectra is a regression problem, where the inputs to the model

https://doi.org/10.1021/acsomega.3c00518
ACS Omega 2023, 8, 14648−14655

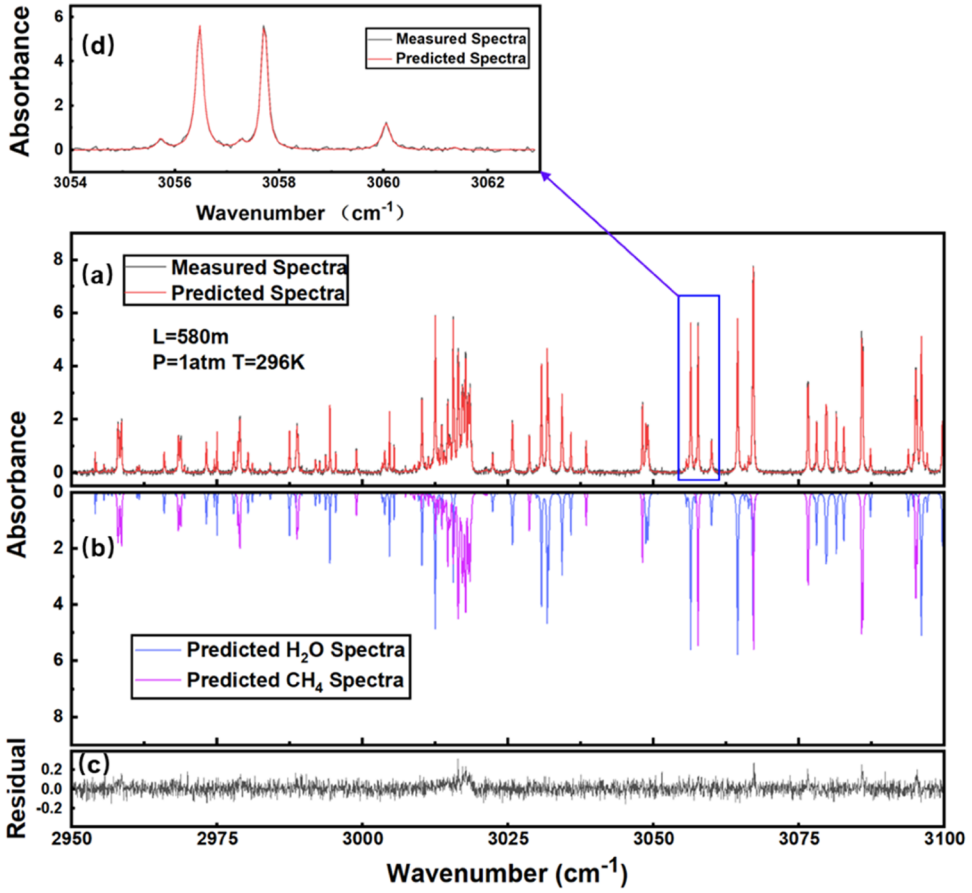

Figure 4. SPM prediction results for 2 ppm methane and 760 ppm water vapor mixture spectra. (a) Experimental and predicted mixed spectra. (b) Individual predicted spectra of methane and water. (c) Residuals between predicted and experimental spectra. (d) Zoomed plot within the range of 3054−3063 cm^{-1}.

are the blended absorption spectra of the dual species and the labels are the respective absorption spectra of the individual gases. The simulated data sets are divided into a 95% training set and a 5% validation set, which are used for tuning the model structure, optimization of the trainable weights, and training hyperparameters. We also experimentally obtained 100 spectra as the test set for the assessment of SPM under real-world situations. The test set is not involved in the training process and is only used as an evaluation of the system performance. The complete development flow is shown in Figure 2.

2.3. Model Architecture and Training Strategy. The architecture of SPM is shown in Figure 3. The input blended spectrum can be expressed as

$$A_s = \sum_{i=1}^{2} (\alpha_i) + N \tag{1}$$

where A_s is the blended spectra with noise and i is the index of the gas component. In the present study, the index 1 is for methane and 2 for water. α_i is the absorption spectrum of the i-th gas, and N is the sum of noises. The SPM consists of two main modules: the feature extraction module of spectral data and the spectral regression module for the spectral separation of individual gases. The SPM is proposed to achieve the separation of the input blended spectrum function and output the individual spectra of the molecular species in the gas mixture, and the underlying function $f_s(\cdot)$ can be expressed as follows

$$\{\hat{\alpha}_1, \hat{\alpha}_2\} = f_s(A_s) \tag{2}$$

$$f_s(A_s) = f_r(f_e(A_s)) \tag{3}$$

where $\hat{\alpha}_1$ and $\hat{\alpha}_2$ represent the separated spectra of methane and water predicted by SPM, and $f_e(\cdot)$ and $f_r(\cdot)$ represent the functions achieved by the feature extraction module and the spectral regression module, respectively. The feature extraction module consists of two convolutional layers followed by a pooling and a batch-normalization layer. The extracted feature information is then aggregated by an attention layer (ECA attention). The previous layer learns and extracts the spectral features and transmits the feature vector to the later layer. The operation of the feature extraction module can be expressed as follows

$$C_{out} = f_e(A_s) \tag{4}$$

where C_{out} is the output feature vector and the ReLU activation function is chosen here. To avoid overfitting due to the large redundancy of data, a pooling layer is added to reduce the computational effort of the model. The final feature vectors are output by the extraction module and subsequently fed forward into the spectral regression module, in which it is mapped to the low-dimensional space to achieve the separation of spectra. The spectral regression module contains three fully connected layers, each of which applies weighted sums of the

https://doi.org/10.1021/acsomega.3c00518
ACS Omega 2023, 8, 14648−14655

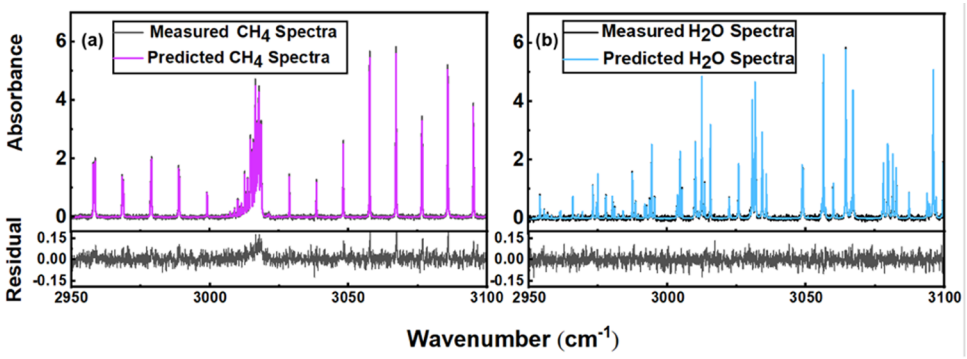

Figure 5. Comparison of measured and predicted spectra of a single gas sample. (a) Measured and predicted methane spectra and their residuals. (b) Measured and predicted water spectra and their residuals.

results from the previous layer and assigns nonlinear factors through the activation function. Its calculation can be expressed as

$$\hat{\alpha}_{out} = f_r(C_{out}) \tag{5}$$

where $\hat{\alpha}_{out} = \{\hat{\alpha}_1, \hat{\alpha}_2\}$ is the set of $\hat{\alpha}_1$ and $\hat{\alpha}_2$. To prevent overfitting, dropout is added in the penultimate layer with dropout rate = 0.3, and the final output of the model is a concatenated spectral vector of individual gases.

We explore extensively the structure of SPM and the setting of hyperparameters. For the model, different combinations of feature extraction modules and spectral regression modules with different structures are explored. Each module structure is determined by starting with a single layer structure and gradually increasing the number of layers to improve its feature learning capability. For the feature extraction module, the size of the convolution kernel is first adjusted to fit the broad spectral data, and then, the number of layers is gradually increased. For the regression module, the effects of different numbers of hidden layers and the neurons in the hidden layer on the model performance are explored. In terms of the training hyperparameters, a certain range of each was explored empirically rather than performing a grid search. For example, for the learning rate, we tried from 10^{-2} to 10^{-7}. However, too small a learning rate may slow down the convergence of the model. To solve this problem, the learning rate decay is finally used. The initial learning rate is 0.01, and the learning rate decays to one-tenth of the original rate at every 2000 epoch interval. In this task, we use the mean square error (MSE) as the loss function with the following expressions

$$\mathrm{MSE} = \frac{1}{m}\sum_{j=1}^{m}(\alpha_{label}^{j} - \hat{\alpha}_{out}^{j})^2 \tag{6}$$

where m is the number of spectra in the data set, and it is 15,000 in the present study. α_{label}^{j} is the ground truth. The optimizer chosen is the Adam optimizer. The entire model was built using the PyTorch framework and the Python 3.7 programming environment. The model was trained on an NVIDIA RTX A5000 GPU for 15,000 epochs. Full code implementation of SPM is available in the Supporting Information.

3. EXPERIMENTAL RESULTS AND ANALYSIS

To verify the generalization performance of SPM under practical conditions, 100 gas mixtures with different concentrations of methane and water vapor were experimentally configured, where the methane was in the range of 0−20 ppm and the water vapor was in the range of 500−3000 ppm. The spectral separation performance of SPM was satisfactory throughout the whole concentration range. Figure 4a shows one presentative prediction of the results with 2 ppm methane and 760 ppm water. The predicted spectrum was synthesized based on the separated spectra and illustrated with the measured one for intuitive comparison. The separated spectra of the individual target gases were inverted as shown in Figure 4b for clarity. Both residuals, which are maintained at low levels throughout the whole spanning range (Figure 4c), and the high agreement of the zoomed range shown in Figure 4d, demonstrate the good performance of SPM. Although the residuals are relatively large in some bands with dense feature absorption peaks, the magnitude was still within the allowable range, demonstrating excellent global realizations. In addition, the experimental measurements inevitably introduce systematic noise, the SPM still performs well and shows strong robustness of noise.

Table 1. Mean AEs of the Predicted Results for Methane and Water of the Top *n* Absorption Feature Screening Mechanism with Respect to the 100 Experimental Spectra

top *n* gas specie	1	2	3	4	5
CH_4 (ppm)	0.0721	0.0712	0.0652	0.0562	0.0698
H_2O (ppm)	12.2538	10.6521	8.6529	7.6531	8.2873

The separated spectra of the individual gases were also compared with their corresponding respectively measured spectra for further verification of separation accuracy. The comparisons were also referred to 2 ppm methane and 760 ppm water. Good agreements were demonstrated for both gases, with the residual under the limits of tolerance (see Figure 5a,b).

The precise separation of blended spectra of SPM allows the system to further achieve the accurate concentration retrieval capability with respect to the target gas methane in the presence of interfering gas water. Considering the potential error of a separated spectrum in the absorption peak, a feature absorption peak screening mechanism was proposed to achieve more accurate concentration retrieval, which avoids the prediction error introduced by only interrogating the individual peaks of the separated spectra. We give full play to the advantages of broadband spectra and use multiple absorption feature peaks to compute the concentration. The top n absorption features in terms of the peak magnitude were leveraged to compute the mean concentration value. The effect

https://doi.org/10.1021/acsomega.3c00518
ACS Omega 2023, 8, 14648−14655

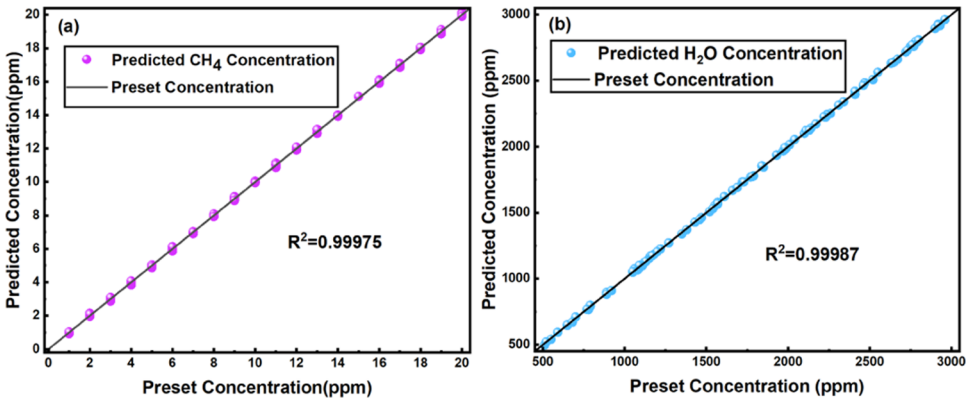

Figure 6. Linear relationship between predicted and preset concentrations: (a) methane and (b) water.

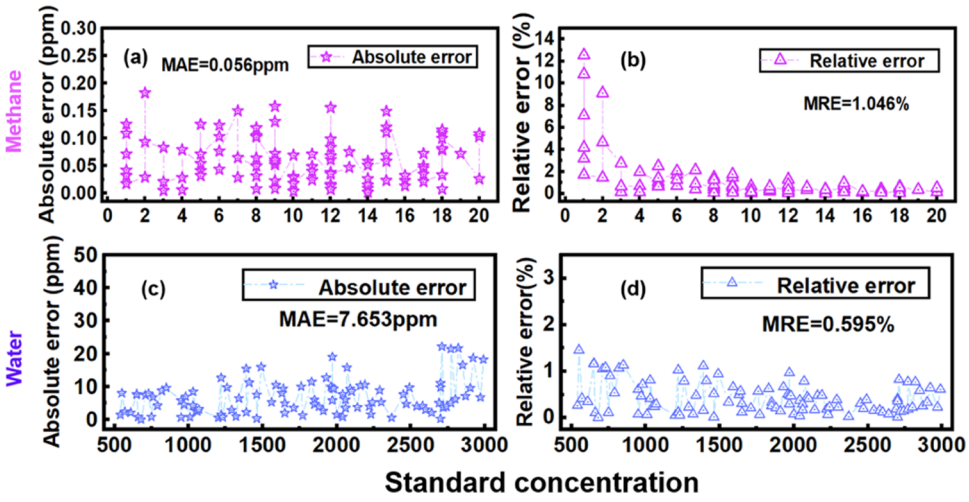

Figure 7. Error analysis of the predicted concentrations. (a) AE of methane. (b) AE of water. (c) RE of methane. (d) RE of water.

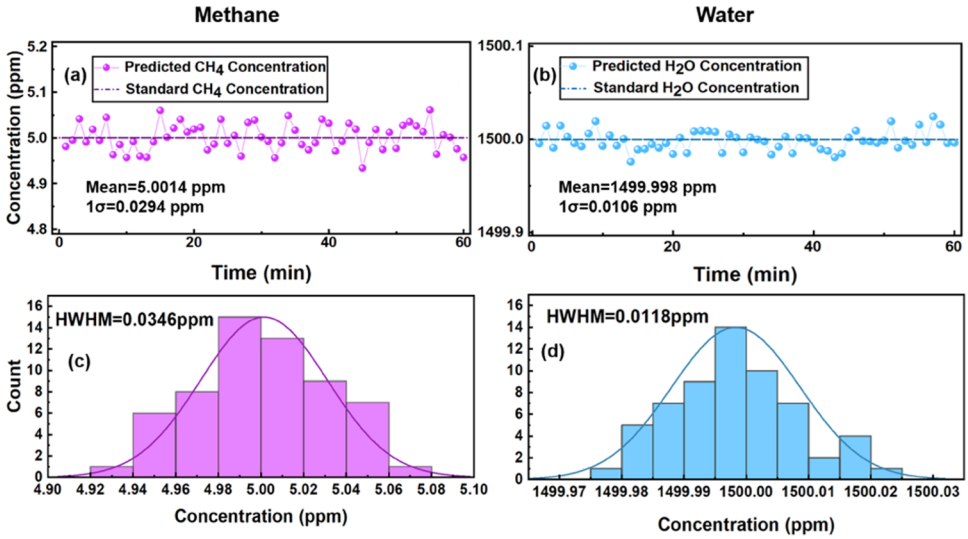

Figure 8. System real-time measurement results. (a) Methane real-time measurement results. (b) Water real-time measurement results. (c) Histogram of statistical distribution of methane real-time measurement results. (d) Histogram of statistical distribution of water real-time measurement results.

of different numbers of selected feature peaks on the predicted concentrations was evaluated and is summarized in Table 1. The best results were derived from the mean concentrations corresponding to the top 4 feature peaks.

The concentrations of methane and water were retrieved based on the top 4 absorption features of the separated spectra. The results are shown in Figure 6. The coefficients of determination reached 0.99975 and 0.99987 for methane and water, respectively, showing a good linear dependence between

https://doi.org/10.1021/acsomega.3c00518
ACS Omega 2023, 8, 14648−14655

the predicted gas concentrations and the standard gas concentration preset by the mass flow controller. The systematic error analysis was also conducted by comparing the two statistical indicators of relative error (RE) and absolute error (AE), as shown in Figure 7. The system maintains stable AEs, and the mean AEs for both species are 0.056 and 7.563 ppm, respectively (Figure 7a,c).

Although the AE of water vapor is higher, it is mainly due to its 2 order of magnitude higher concentration level compared with that of methane, and the overall performance can still meet the needs of most applications. In terms of REs, the mean REs for methane and water vapor were 1.046 and 0.595%, respectively. The RE of water is stable throughout the whole concentration range (Figure 7d), while the RE of methane increased with the decrease of concentration (Figure 7b). This may be due to the more complex spectral structure of methane compared to water within the selected spectral window and the relatively low signal-to-noise ratio of methane spectra at lower concentrations. This problem can be subsequently, in general, be eliminated by means of active real-time filtering.

To assess the long-term detection stability of the proposed system, the customized gas mixture with 5 ppm methane and 1500 ppm water vapor was injected into the gas cell. The real-time detection was carried out at the ambient pressure of 1 atm and temperature of 296 K. During the one-hour experiment, each prediction was retrieved at one-minute intervals. The results demonstrated the good stability of the system as shown in Figure 8. The mean predictions were 5.0014 ppm and 1499.998 ppm for methane and water, respectively. The statistical histograms can be well fitted by Gaussian distribution with half-width at half-maximum (HWHM) values of 0.0346 and 0.0118 ppm, respectively, as shown in Figure 8c,d. The results show that the SPM enhanced broadband MIR dual-comb spectrometer can achieve stable measurement in real-time detections. The detection column densities for methane and water vapor were 17.052 and 6.148 ppm-m, respectively. The absorptions of methane and water are widely spread and overlapped within the selected spectral window; therefore, the successful decoupling of our system to blended absorption spectra demonstrates the potential feasibility of applying such a method to other gas mixtures.

4. CONCLUSIONS

In general, we have developed a dual-comb spectrometer integrated with a neural network-based spectral decoupling algorithm for the simultaneous detection of a methane and water gas mixture. The system features the broadband dual frequency comb laser source in conjunction with a multipass cell to realize high sensitivity and quality of spectra data. A novel deep learning model, referred to as SPM, was proposed to achieve the precise spectral separation of the target gas methane from the interference gas water. In addition, to achieve more accurate concentration retrieval from the separated spectra, a feature absorption peak screening mechanism was proposed, which avoids the prediction error introduced by only interrogating the individual peaks of the separated spectra. Subsequently, the feasibility of SPM in practical detection applications is verified by evaluating the systematic error and long-term detection stability. The successful decoupling of the blended absorption spectra of methane and water shows that the proposed method can effectively solve the cross-interference problem in the blended spectra and demonstrates the underlying feasibility for spectral decoupling to other gas mixtures.

Although the performance of SPM was validated for mixtures of methane and water, the current SPM is still a prototype. The performance of SPM in a wider range of gas mixtures remains to be validated. Based on the successes of deep learning in concentration retrieval and gas prediction in the field of absorption spectroscopy, we believe that deep learning can effectively contribute to the research of sensing and decoupling of multicomponent gas mixtures. Therefore, we will continue working in decoupling of multicomponent gas mixtures in massive paralleling molecular sensing in our future research.

■ ASSOCIATED CONTENT

Supporting Information

The Supporting Information is available free of charge at https://pubs.acs.org/doi/10.1021/acsomega.3c00518.

Full code implementation for all algorithms (PDF)

■ AUTHOR INFORMATION

Corresponding Authors

Linbo Tian − *Key Laboratory of Education Ministry for Laser and Infrared System Integration Technology, Shandong University, Qingdao 266237, China; Shandong Provincial Key Laboratory of Laser Technology and Application, Shandong University, Qingdao 266237, China;* orcid.org/0000-0003-2399-1727; Email: linbotian@mail.sdu.edu.cn

Sasa Zhang − *School of Information Science and Engineering, Shandong University, Qingdao 266237, China; Key Laboratory of Education Ministry for Laser and Infrared System Integration Technology, Shandong University, Qingdao 266237, China; Shandong Provincial Key Laboratory of Laser Technology and Application, Shandong University, Qingdao 266237, China;* orcid.org/0000-0002-0568-3803; Email: sasazhang@sdu.edu.cn

Authors

Qingjin Chi − *School of Information Science and Engineering, Shandong University, Qingdao 266237, China; Shandong Provincial Key Laboratory of Laser Technology and Application, Shandong University, Qingdao 266237, China;* orcid.org/0000-0002-7792-8769

Rongqi Xu − *Key Laboratory of Education Ministry for Laser and Infrared System Integration Technology, Shandong University, Qingdao 266237, China; Shandong Provincial Key Laboratory of Laser Technology and Application, Shandong University, Qingdao 266237, China*

Zhao Wang − *Key Laboratory of Education Ministry for Laser and Infrared System Integration Technology, Shandong University, Qingdao 266237, China; Shandong Provincial Key Laboratory of Laser Technology and Application, Shandong University, Qingdao 266237, China*

Fengrong Zhao − *School of Information Science and Engineering, Shandong University, Qingdao 266237, China; Shandong Provincial Key Laboratory of Laser Technology and Application, Shandong University, Qingdao 266237, China*

Kegang Guo − *School of Information Science and Engineering, Shandong University, Qingdao 266237, China; Shandong Provincial Key Laboratory of Laser Technology and Application, Shandong University, Qingdao 266237, China*

https://doi.org/10.1021/acsomega.3c00518
ACS Omega 2023, 8, 14648−14655

Zhaowen Liang − *School of Mechanical Engineering, Beijing Institute of Technology, Beijing 100081, China*
Jinbao Xia − *State Key Laboratory of Crystal Materials, Shandong University, Jinan 250100, China; The State Key Laboratory of Applied Optics, Changchun 130000, China*

Complete contact information is available at: https://pubs.acs.org/10.1021/acsomega.3c00518

Author Contributions

Q.C.: Conceptualization, investigation, writing—original draft, methodology, software. L.T.: Supervision, writing—review & editing, software. R.X.: Writing—review & editing, software. Z.W.: writing—review & editing. F.Z.: Writing—review & editing. K.G.: Writing—review & editing. Z.L.: Writing—review & editing. J.X.: Writing—review & editing. S.Z.: Supervision, funding acquisition, project administration.

Notes

The authors declare no competing financial interest.

■ ACKNOWLEDGMENTS

This work was supported by the National Natural Science Foundation of China (61475085), the Key Research and Development Program of Shandong Province (no. 2020CXGC010104), Qingdao science and technology demonstration and guidance project (no. 21-1-4-sf-1-nsh), Open Fund of State Key Laboratory of Applied Optics (SKLA02020001A12), and the Robert A. Welch Foundation (Grant no. A1546).

■ REFERENCES

(1) Wittstock, V.; Scholz, L.; Bierer, B.; Perez, A. O.; Wöllenstein, J.; Palzer, S. Design of a LED-based sensor for monitoring the lower explosion limit of methane. *Sens. Actuators, B* **2017**, *247*, 930−939.
(2) Shi, L.; Wang, J.; Zhang, G.; Cheng, X.; Zhao, X. A risk assessment method to quantitatively investigate the methane explosion in underground coal mine. *Process Saf. Environ. Prot.* **2017**, *107*, 317−333.
(3) Niu, M. Y.; Liang, W. Y.; Wang, F. P. Methane biotransformation in the ocean and its effects on climate change: A review. *Sci. China: Earth Sci.* **2018**, *61*, 1697−1713.
(4) He, L.; Fan, Y. L.; Bellettre, J.; Yue, J.; Luo, L. G. A review on catalytic methane combustion at low temperatures: Catalysts, mechanisms, reaction conditions and reactor designs. *Renewable Sustainable Energy Rev.* **2020**, *119*, 109589.
(5) Arminio-Ravelo, J. A.; Escudero-Escribano, M. Strategies toward the sustainable electrochemical oxidation of methane to methanol. *Curr. Opin. Green Sustainable Chem.* **2021**, *30*, No. 100489.
(6) Li, D. L.; Du, J. W.; He, S.; Liang, D. Q.; Zhao, X. Y.; Yang, X. Y. Measurement and modeling of the effective thermal conductivity for porous methane hydrate samples. *Sci. China: Chem.* **2012**, *55*, 373−379.
(7) Tian, L. B.; Sun, J. C.; Chang, J.; Xia, J. B.; Zhang, Z. F.; Kolomenskii, A. A.; Schuessler, H. A.; Zhang, S. S. Retrieval of gas concentrations in optical spectroscopy with deep learning. *Measurement* **2021**, *182*, 109739.
(8) Tian, L. B.; Sun, J. C.; Zhang, S. S.; Kolomenskii, A. A.; Schuessler, H. A.; Wang, Z.; Xia, J. B.; Chang, J.; Liu, Z. J. Near-infrared methane sensor with neural network filtering. *Sens. Actuators, B* **2022**, *354*, 131207.
(9) Hodgkinson, J.; Tatam, R. P. Optical gas sensing: a review. *Meas. Sci. Technol.* **2013**, *24* (1), 012004.
(10) Deng, B. T.; Sima, C.; Xiao, Y. F.; Wang, X. F.; Ai, Y.; Li, T. L.; Lu, P.; Liu, D. M. Modified laser scanning technique in wavelength modulation spectroscopy for advanced TDLAS gas sensing. *Opt. Lasers Eng.* **2022**, *151*, 106906.
(11) Chen, T.-L.; Ober, D. C.; Miri, R.; Bui, T. Q.; Shen, L. H.; Okumura, M. Optically Switched Dual-Wavelength Cavity Ring-Down Spectrometer for High-Precision Isotope Ratio Measurements of Methane delta D in the Near Infrared. *Anal. Chem.* **2021**, *93*, 6375−6384.
(12) Zhou, J.; Er, Z. X.; Gong, P.; Xie, L.; Jiang, X. K. A compact gas monitoring system for methane based on photoacoustic spectroscopy. *Infrared Phys. Technol.* **2022**, *123*, 104186.
(13) Xiao, H. K.; Levine, S. P.; Darcy, J. B. Iterative Least-Squares Fit procedures for the identification of organic vapor mixtures by fourier-transform infrared spectrophotometry. *Anal. Chem.* **1989**, *61*, 2708−2714.
(14) Genner, A.; Martin-Mateos, P.; Moser, H.; Lendl, B. A Quantum Cascade Laser-Based Multi-Gas Sensor for Ambient Air Monitoring. *Sensors* **2020**, *20*, No. 1850.
(15) Hay, K. G.; Wright, S.; Duxbury, G.; Langford, N. In-flight measurements of ambient methane, nitrous oxide and water using a quantum cascade laser based spectrometer. *Appl. Phys. B: Lasers Opt.* **2008**, *90*, 329−337.
(16) Li, L.; Chen, Y.; Wu, S.; Jiang, L.; Cheng, Y. A Rapid Gas Chromatography Method for Determination of Methane in Water Sample. *Environ. Sci. Technol.* **2018**, *41*, 143−148.
(17) Mastny, E. A.; Miller, C. A.; de Pablo, J. J. The effect of the water/methane interface on methane hydrate cages: The potential of mean force and cage lifetimes. *J. Chem. Phys.* **2008**, *129*, 034701.
(18) Yang, X.; Xie, Z.; Li, Y.; Zhang, Y. Enantioselective aerobic oxidative cross-dehydrogenative coupling of glycine derivatives with ketones and aldehydes via cooperative photoredox catalysis and organocatalysis. *Chem. Sci.* **2020**, *11*, 4741−4746.
(19) Sun, Y. W.; Zeng, Y.; Liu, W. Q.; Xie, P. H.; Chan, K. L.; Li, X. X.; Wang, S. M.; Huang, S. H. Cross-interference correction and simultaneous multi-gas analysis based on infrared absorption. *Chin. Phys. B* **2012**, *21*, 090701.
(20) Smid, S. C.; McNeish, D.; Miocevic, M.; van de Schoot, R. Bayesian Versus Frequentist Estimation for Structural Equation Models in Small Sample Contexts: A Systematic Review. *Struct. Equation Modeling* **2020**, *27*, 131−161.
(21) Bro, R.; Smilde, A. K. Principal component analysis. *Anal. Methods* **2014**, *6*, 2812−2831.
(22) Stanley, T. D.; Doucouliagos, H. Neither fixed nor random: weighted least squares meta-analysis. *Stat. Med.* **2015**, *34*, 2116−2127.
(23) Benitez, J.; Henseler, J.; Castillo, A.; Schuberth, F. How to perform and report an impactful analysis using partial least squares: Guidelines for confirmatory and explanatory IS research. *Inf. Manage.* **2020**, *57*, 103168.
(24) Dong, S.; Wang, P.; Abbas, K. A survey on deep learning and its applications. *Comput. Sci. Rev.* **2021**, *40*, 100379.
(25) Benton, E. N.; Perera, N. A. K. R.; Nesterov, V. N.; Perera, W.; Omary, M. A.; Marpu, S. B. A Europium-Based Optical Sensor for the Detection of Carbon Dioxide and Its Application for a Fermentation Reaction. *Chemosensors* **2023**, *11*, 5.
(26) Sun, J.; Tian, L.; Chang, J.; Kolomenskii, A. A.; Schuessler, H. A.; Xia, J.; Feng, C.; Zhang, S. Adaptively Optimized Gas Analysis Model with Deep Learning for Near-Infrared Methane Sensors. *Anal. Chem.* **2022**, *94*, 2321−2332.
(27) Venkatesan, R.; Prabu, S. Hyperspectral Image Features Classification Using Deep Learning Recurrent Neural Networks. *J. Med. Syst.* **2019**, *43*, 216.